Proceedings of the ASME 2011 Pressure Vessels & Piping Division Conference
PVP2011
July 17-21, 2011, Baltimore, Maryland, USA

PVP2011-57471

COMPUTATION OF LOW REYNOLDS NUMBER FLOW AROUND A CIRCULAR CYLINDER FOLLOWING A HORSESHOE-SHAPED PATH

László Baranyi
Department of Fluid and Heat Engineering, University of Miskolc
3515 Miskolc-Egyetemváros, Hungary
arambl@uni-miskolc.hu

ABSTRACT

Two-degree-of-freedom vortex-induced vibration investigations of low-mass ratio circular cylinders show that the streamwise frequency of oscillations is about twice that of the transverse oscillation. These cylinders have been observed to trace Lissajous-type trajectories. Depending on the phase difference between in-line and transverse motions paths, different shapes can be obtained, such as trajectories resembling a figure 8 or a horseshoe.

In this study low Reynolds number flow is investigated numerically for a cylinder placed in a uniform stream and forced to follow a horseshoe-like path. Investigations were carried out using a thoroughly tested finite difference code developed by the present author.

The mechanical energy transfer between the fluid and the cylinder, time-mean and rms values of force coefficients are investigated. Computations are carried out for Reynolds numbers of Re=140, 200 and 250 in the lock-in domain against the frequency ratio while other parameters are kept constant. All investigations were carried out at two phase difference values, resulting in convex and concave arc paths called horseshoe-shaped paths.

The mechanical energy transfer and the time-mean and rms values of force coefficients show that a sudden jump in values is often observed, affecting flow features. Positive energy transfer after the jump is common.

Keywords: forced cylinder motion, low Reynolds number, two-degree-of-freedom motion, vortex shedding

INTRODUCTION

The flow past a single oscillating cylinder has been studied by various researchers at both high and low Reynolds numbers. Both experimental and numerical studies have dealt with pure transverse cylinder motion (e.g., Williamson and Roshko, 1988; Lu and Dalton, 1996; Blackburn and Henderson, 1999) or pure in-line cylinder motion (e.g., Cetiner and Rockwell, 2001; Al-Mdallal et al., 2007; Mureithi et al., 2010). However, far fewer investigations have been carried out for two-degree-of-freedom (2-DoF) cylinder motion.

Experience shows (see e.g., Kheirkhah and Yarusevych, 2010) that where the mass ratio (the ratio of the mass of the displaced fluid to the mass of the vibrating system) is high, as mainly occurs when a structure is oscillating in air, then the frequency of oscillation in in-line and in transverse directions are approximately equal to each other. This can lead to an elliptical path, such as that observed in tube bundles in heat exchangers. Elliptical cylinder motion studies include Didier and Borges (2007), Baranyi (2008) and Kheirkhah and Yarusevych (2010).

With a low mass ratio, typically found when a cylinder is moving in liquid, the frequency of the cylinder motion in in-line direction is approximately twice its frequency in transverse direction, as found by Jeon and Gharib (2001), Jauvtis and Williamson (2004), Flemming and Williamson (2005), Leong and Wei (2008) and Sanchis et al. (2008). For a cylinder in motion, this can also be the case; thus, cables and pipes submersed in flowing water may experience this kind of motion. The vortex-induced vibration (VIV) arising in this way can lead to problems such as fatigue and damage of structures.

When the in-line cylinder motion frequency is twice the frequency of transverse cylinder motion, the phase difference between in-line and transverse motion appears to be responsible for different cylinder paths (e.g., Sanchis et al., 2008). One observed case is a figure-eight-shaped path, while a path in the shape of an arc, or C-shape, has also been observed in the experimental study for an elastically supported cylinder of Sanchis et al. (2008) in the Reynolds number domain of

Re=(1.3 to 1.9)x10^4 and in the numerical work of Prasanth and Mittal (2009). The latter investigated flow-induced vibration of two elastically supported cylinders in tandem arrangement. They found that at low reduced velocity the lobes of the figure-eight-shape path are very thin and bent downstream, appearing almost like arcs. While figure-eight paths have been studied to some extent (e.g., Baranyi, 2010; Peppa et al., 2010), to the best of my knowledge the arc-shaped path – which I shall call a horseshoe path – has not been investigated further. Jeon and Gharib (2001) in their experimental study of flow around a forced 2-DoF cylinder motion investigated regular figure-eight paths and figure-eight patterns with the lobes bent slightly downstream.

Investigation of a cylinder following a horseshoe path is interesting not only for a more thorough knowledge of flow behavior and vortex shedding, but because it is relevant to the design of underwater structures and the understanding of the vortex-induced vibration that can lead to their fatigue or failure.

Here, forced oscillation will be used to simulate flow around a cylinder and to shed some light on stability behavior as a preliminary study, without carrying out a full fluid-structure interaction (FSI) study at this time. While a direct relationship is difficult to ascertain between results of investigations of free and of forced vibration (e.g., Williamson, 2004), this is a first step towards considering FSI, especially in terms of mechanical energy transfer between cylinder and fluid.

In this numerical study a circular cylinder is placed in a uniform flow and mechanically oscillated simultaneously in two directions, yielding a horseshoe-like path (either convex or concave), for three low Reynolds numbers. Energy transfer and the time-mean and rms values of force coefficients are also investigated.

NOMENCLATURE

$a_{0x,y}$ dimensionless x and y components of cylinder acceleration
$A_{x,y}$ amplitude of oscillation in x or y directions, respectively, non-dimensionalized by d
C_D drag coefficient, $2F_D/(\rho U^2 d)$
C_L lift coefficient, $2F_L/(\rho U^2 d)$
d cylinder diameter (m)
E mechanical energy transfer
f oscillation frequency, non-dimensionalized by U/d
f_v vortex shedding frequency, non-dimensionalized by U/d
p pressure, non-dimensionalized by ρU^2
R radius, non-dimensionalized by d
Re Reynolds number, Ud/ν
St non-dimensional vortex shedding frequency, $f_v d/U$
t time, non-dimensionalized by d/U
tq torque coefficient, torque of shear on cylinder surface, non-dimensionalized by $\rho U^2 d^2$
U free stream velocity, velocity scale (m/s)
x,y Cartesian coordinates, non-dimensionalized by d

Subscripts

D drag
fb fixed body
L lift
rms root-mean-square value
v vortex shedding
x, y components in x and y directions
0 for cylinder motion; for stationary cylinder at same Re
1 on the cylinder surface; for energy transfer in transverse direction
2 on the outer boundary of the physical domain; for energy transfer in in-line direction

COMPUTATIONAL METHOD

A non-inertial system fixed to the accelerating cylinder is used to compute 2D low-Reynolds number unsteady flow around a circular cylinder placed in a uniform stream and forced to oscillate in transverse, in in-line direction, or both. The non-dimensional Navier-Stokes equations for incompressible constant-property Newtonian fluid, the equation of continuity and the Poisson equation for pressure can be written as follows:

$$\frac{\partial u}{\partial t}+u\frac{\partial u}{\partial x}+v\frac{\partial u}{\partial y}=-\frac{\partial p}{\partial x}+\frac{1}{\mathrm{Re}}\nabla^2 u-a_{0x} \tag{1}$$

$$\frac{\partial v}{\partial t}+u\frac{\partial v}{\partial x}+v\frac{\partial v}{\partial y}=-\frac{\partial p}{\partial y}+\frac{1}{\mathrm{Re}}\nabla^2 v-a_{0y} \tag{2}$$

$$D=\frac{\partial u}{\partial x}+\frac{\partial v}{\partial y}=0 \tag{3}$$

$$\frac{\partial^2 p}{\partial x^2}+\frac{\partial^2 p}{\partial y^2}=2\left[\frac{\partial u}{\partial x}\frac{\partial v}{\partial y}-\frac{\partial u}{\partial y}\frac{\partial v}{\partial x}\right]-\frac{\partial D}{\partial t} \tag{4}$$

In these equations, u and v are the x and y components of velocity, t is time, p is the pressure, Re is the Reynolds number based on cylinder diameter d, free stream velocity U, and kinematic viscosity ν, and D is the dilation. Although D is theoretically equal to 0 from equation (3), it is kept in equation (4) to avoid accumulation of numerical errors. In equations (1) and (2) a_{0x} and a_{0y} mean the x and y components of cylinder acceleration, respectively.

On the cylinder surface, no-slip boundary condition is used for the velocity and a Neumann type boundary condition is used for the pressure. At the far region, potential flow is assumed. Computational results show that this approximation results in some inaccuracies near the outer boundary only, and in practice it has no influence on the results of the near-wake flow and forces acting on the cylinder.

Boundary-fitted coordinates are used to impose the boundary conditions accurately. The physical domain bounded by two concentric circles is mapped into a rectangular computational domain with equidistant spacing in both directions (see Fig. 1). In the physical domain logarithmically spaced radial cells are used, providing a fine grid scale near the cylinder wall and a coarse grid in the far field. The transformed governing equations and boundary conditions are solved by finite difference method. Space derivatives are approximated by fourth order central differences, except for the convective terms

for which a third order modified upwind scheme is used. The Poisson equation for pressure is solved by the successive over-relaxation (SOR) method. The Navier-Stokes equations are integrated explicitly and continuity is satisfied at every time step. For further details see Baranyi (2003; 2008).

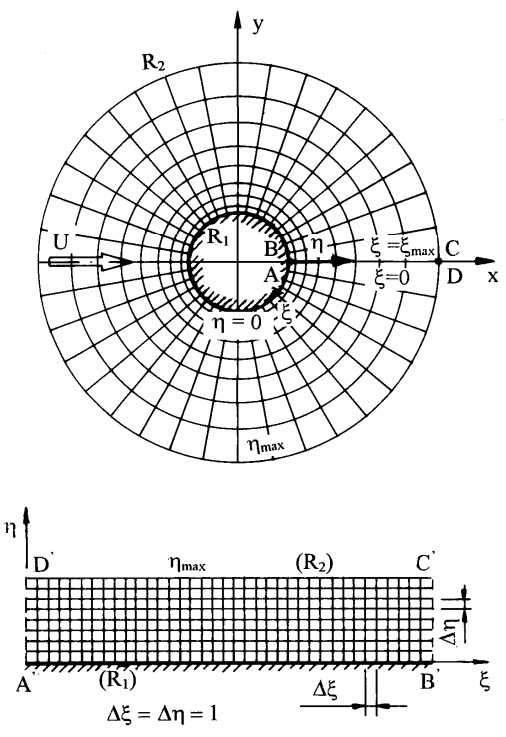

Figure 1. Physical and computational domains

The 2D code developed by the author has been extensively tested against experimental and computational results for a stationary cylinder and computational results for cylinders oscillating in transverse or in in-line directions or following a circular path, including Lu and Dalton (1996), Al-Mdallal et al. (2007), and Didier and Borges (2007), with good agreement being found, (Baranyi, 2008). For the majority of computations in this study the dimensionless time step is 0.0005, the number of grid points is 481x451, and a relatively large physical domain of R_2/R_1=360 has been chosen to enhance accuracy.

This study investigates the behavior of flow past a cylinder placed in a uniform stream with its axis perpendicular to the main flow. The cylinder is oscillated mechanically in both in-line and transverse directions in relation to the uniform stream. The dimensionless cylinder displacement is described by the following equations:

$$x_0=A_x \sin(2\pi f_x t+\Theta)\,, \tag{5}$$

$$y_0= A_y \sin(2\pi f_y t)\,, \tag{6}$$

where Θ is the relative phase angle between the streamwise and transverse motion. Different phase angle values result in different cylinder paths. Θ =0 gives a symmetric figure-8-path; when $\Theta = -\pi/4$ the path is a figure-8-pattern with the lobes bent slightly downstream. If we decrease the value of Θ further in the interval of $-\pi/2 < \Theta < -\pi/4$ the lobes of figure 8 become thinner, and their thickness disappears completely in the limiting case of $\Theta = -\pi/2$, resulting in a convex path which I will call a horseshoe path in the paper. When $\Theta = \pi/2$ the resulting path is a concave curve – the mirror image around the vertical axis of the convex curve belonging to $\Theta = -\pi/2$. Naturally in Eqs. (5) and (6) the second time derivatives of x_0 and y_0 give the accelerations a_{0x} and a_{0y} in equations (1) and (2). The dimensionless oscillation amplitudes in this study are fixed at A_x=0.1 and A_y=0.4, ensuring slender cylinder paths. Although initial condition was earlier found to influence the number and/or location of jumps (Baranyi, 2008), this has not been investigated here.

The time-history of force coefficients (lift, drag, base pressure and torque), pressure and velocity field are computed. From these data, time-mean (TM) and root-mean-square (rms) values of force coefficients, streamlines, and vorticity contours can be obtained.

Throughout this paper the lift and drag coefficients used do not contain the inertial forces originated from the non-inertial system fixed to the accelerating cylinder. Coefficients obtained by removing the inertial forces are often termed 'fixed body' coefficients (see Lu and Dalton, 1996). The relationship between the two sets of coefficients can be written as

$$C_D=C_{D\,fb}+\pi\, a_{0x}/2, \tag{7}$$

$$C_L=C_{L\,fb}+\pi\, a_{0y}/2, \tag{8}$$

where subscript 'fb' refers to the fixed body (understood in an inertial system fixed to the stationary cylinder), Baranyi (2005). Since the inertial terms are periodic functions, their time-mean values vanish, resulting in identical TM values for lift and drag in the inertial and non-inertial systems. Naturally the rms values of C_L and C_D will be somewhat different in the two systems (but this does not affect the curve being continuous).

Investigation was restricted to lock-in cases. Lock-in, or the synchronization between vortex shedding and cylinder motion, produces a periodic solution for each of the force coefficients. In this paper, we consider lock-in to be when the vortex shedding frequency is identical to f_y, the frequency of transverse cylinder oscillation.

Jeon and Gharib (2001) suggest that the value of phase angle Θ tends to drift for free-vibration cases, but is usually in the range of 0 to – 45°. Θ=0° corresponds to figure-eight motion, while – 45° of phase results in a figure-eight pattern with the lobes bent slightly downstream. However, when looking at the results of Sanchis et al. (2008) and those of Prasanth and Mittal (2009) at low reduced velocity values, the width of the lobes of the bent figure-eight paths is almost zero, practically yielding a *convex* arc when viewed from upstream. Equation (5) yields this path at $\Theta = -\pi/2$. In addition, the case of $\Theta = \pi/2$ is also investigated, yielding a *concave* path, which is the mirror image of the convex path with respect to axis *y*. The author admits that at present the latter case might not have much practical importance.

To create a *convex* or *concave* cylinder path (when the path is viewed from upstream of the cylinder), the values of

$$\textit{Convex}\ \text{path:} \qquad f_x=2\,f_y; \quad \Theta = -\,\pi/2, \tag{9}$$

$$\textit{Concave}\ \text{path:} \qquad f_x=2\,f_y; \quad \Theta = \pi/2 \tag{10}$$

are substituted into Eqs. (5) and (6). The two paths are shown in Fig. 2.

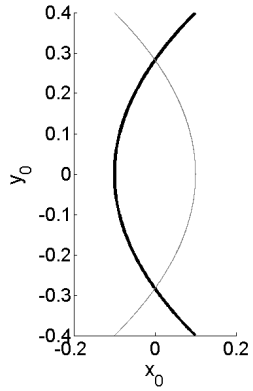

Figure 2. Convex (thick line) and concave (thin line) cylinder paths

The non-dimensional mechanical energy transfer originally introduced by Blackburn and Henderson (1999) for transversely oscillated cylinder was extended for a general 2-DoF motion of the cylinder by Baranyi (2008):

$$E=\frac{2}{rU^2d^2}\int_0^T \mathbf{F}\cdot\mathbf{v}_0\,\mathrm{d}t=\int_0^T\left(C_D\,v_{0x}+C_L\,v_{0y}\right)\mathrm{d}t\,, \tag{11}$$

where T is the motion period, v_{0x} and v_{0y} are the velocity of the cylinder in x and y directions, respectively. Since in this case the dimensionless frequencies are different in the two directions;

$$f_x=2f_y,$$

there exist two periods of

$$T_x=1/f_x \quad \text{and} \quad T=T_y=1/f_y=2T_x. \tag{12}$$

As seen in Eq. (12) the larger period of T_y is used in Eq. (11). For transverse cylinder oscillation $x_0=0$, hence only the integral of the product of lift and transverse cylinder velocity component contributes to the energy transfer. This will be denoted by E_1, and that originating from the drag and in-line cylinder velocity component by E_2. In the general 2-DoF case both E_1 and E_2 are different from zero. The sum of E_1 and E_2 gives the mechanical energy transfer $E= E_1 + E$.

RESULTS

In this study, computations are carried out for the convex and concave cylinder paths for Reynolds numbers of Re=140, 200 and 250 against frequency ratio f_y/St_0 within the synchronization or lock-in domain. Mechanical energy transfer E between the cylinder and the fluid, time-mean (TM) and rms values of lift C_L, drag C_D, base pressure C_{pb} and torque tq coefficients are investigated but for the sake of simplicity only C_L, C_D and E values will be shown in the paper. Sudden jumps between state curves were found in some cases; these indicate a sudden change in the vortex structure (Blackburn and Henderson, 1999; Baranyi, 2008). Values just before and just after a jump are presented in a pre- and post-jump analysis. In addition, for Re=140 results are presented for two domain sizes.

Comparison of Results for Two Domains

Computations were carried out for two computational domains very different in size for both convex and concave paths for Re=140. The smaller domain is characterized by the ratio of outer radius to cylinder radius of R_2/R_1=60 (see Fig. 1) and mesh points of 360 x 236, and the large one by R_2/R_1=360 and 480 x 451 (finer mesh), respectively.

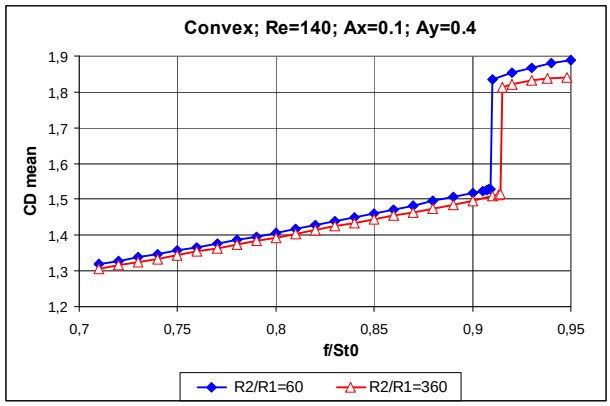

Figure 3. Time-mean value of drag against frequency ratio (filled diamonds: R_2/R_1=60; empty triangles: R_2/R_1=360)

Due to lack of space examples are shown only for the convex cylinder path. Figures 3 to 5 use the same symbols: filled diamonds for the smaller domain and empty triangles for the larger computational domain. Figure 3 shows the TM of drag for the two domains versus frequency ratio. It can be seen that, in spite of the large difference in the domain sizes and the difference in the mesh quality, the two solutions compare relatively well. The discrepancy between the two curves is somewhat higher at higher frequency ratio values. The jump in the solution occurs at around f/St_0=0.91 for both cases. St_0=0.1805 was used for Re=140.

Figures 4 and 5 show the rms of (fixed body) lift and mechanical energy transfer E for the two domains against frequency ratio, respectively. Almost perfect agreement is found between the curves below f/St_0=0.91 in both figures and the jump is reproduced by both methods. It is worthwhile to note that energy transfer E is negative

below the jump at around f/St_0=0.91, meaning that energy is extracted from the cylinder and the fluid acts against the cylinder motion. Above the jump, however, E becomes positive, which means that the cylinder obtains energy from the fluid and that the fluid amplifies the cylinder motion. In free-vibration cases this would mean vortex-induced vibration (VIV).

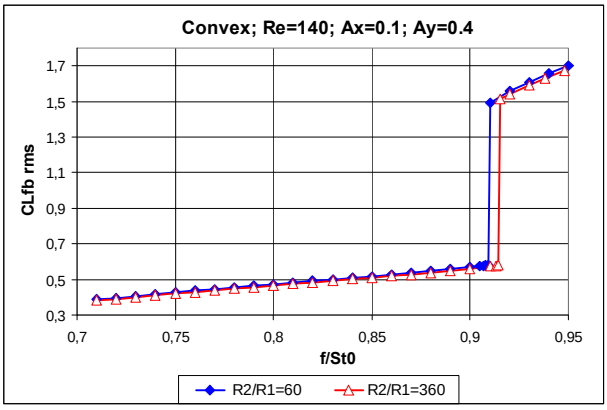

Figure 4. Rms value of fixed body lift against frequency ratio (filled diamonds: R_2/R_1=60; empty triangles: R_2/R_1=360)

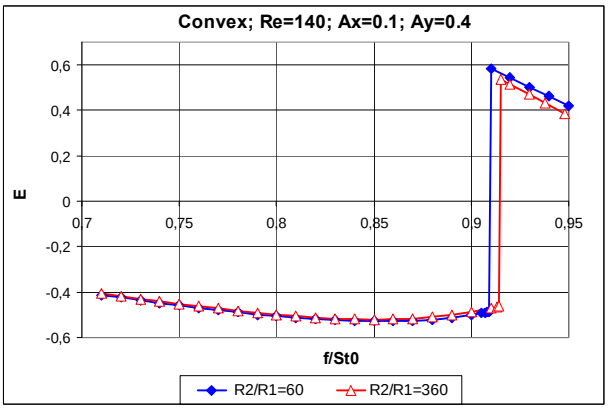

Figure 5. Energy transfer against frequency ratio (filled diamonds: R_2/R_1=60; empty triangles: R_2/R_1=360)

Differences in the results due to different domain sizes (and mesh) obtained for the concave cylinder paths (not shown here) were similar to the cases shown here. Although the results for the small and large computational domains compare well for both types of cylinder path, in aiming to obtain reliable and accurate solution, even at high computational cost, it was decided to use the larger computational domain with R_2/R_1=360 and a fine mesh of 480 x 451.

Results for Convex Cylinder Paths

Mechanical energy transfer and TM and rms values of fixed body lift and drag coefficients were systematically investigated over the lock-in frequency ratio domain for the three Reynolds numbers of Re=140, 200 and 250 for the convex cylinder path. The corresponding dimensionless vortex shedding frequencies St_0 from a stationary cylinder at these Reynolds numbers are 0.1806, 0.1954 and 0.2035 (Posdziech and Grundmann, 2007).

The TM values of fixed body lift were found to be basically zero over the investigated frequency ratio domain for all three Reynolds numbers. That is the reason why they are not shown here. Figure 6 shows the rms values of fixed body lift versus f_y/St_0 for the three Reynolds numbers. We can see one jump for each Re. These jumps are probably caused by sudden switches in the vortex structure (see e.g., Blackburn and Henderson, 1999; Baranyi, 2008). The location of the jumps shifts to smaller frequency values and the width of the lock-in domain decreases with increasing Reynolds number. As can be seen in the figure there are substantial differences between pre- and post-jump values of rms of lift. The state curves were found to be symmetric around zero (i.e., the value for a stationary cylinder) for in-line oscillation (Baranyi, 2009), and this may be the case here, as well. If so, it is probably due to a symmetry-breaking bifurcation (see e.g., Crawford and Knobloch, 1991).

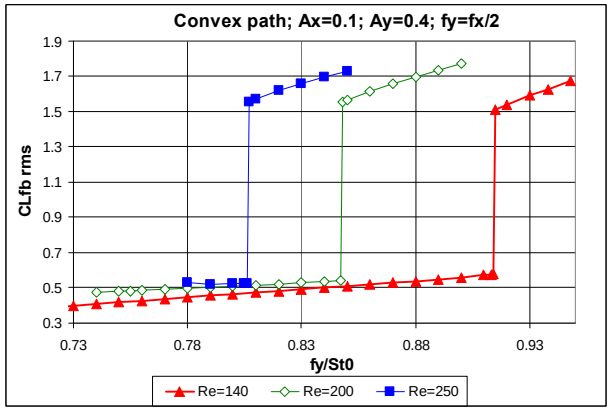

Figure 6. Rms of fixed body lift versus frequency ratio for Re=140, 200 and 250

Figure 7 shows the TM of fixed body drag and looks quite similar to Fig. 6. The drag coefficients increase gradually with the frequency ratio until the jumps occur; afterwards the line becomes curved. As can be seen in Fig. 7, again there are substantial differences between pre- and post-jump values of TM of drag. Figure 8 shows the rms of fixed body drag versus frequency ratio. The state curves in this figure look almost like the complements of those shown in Figs. 6 and 7. It can also be observed in the figure that the relationship between the rms values and the frequency ratio is almost linear before and after the jump for all three Re values. As expected, the rms value of drag increases with f_y/St_0.

Figure 9 shows the mechanical energy transfer E between the fluid and cylinder versus frequency ratio. As can be seen in the figure, E is negative before the jumps for all three Re values. This means that energy is extracted from the cylinder, so the fluid would dampen the cylinder motion in the case of free vibration. However, the sign of E changes to positive after the jump for all Reynolds numbers, meaning that energy is added to

the cylinder. This situation might cause VIV in the case of free vibration. It is to be noted that the location and number of jumps are identical in Figs. 6 to 9 for all three Re values.

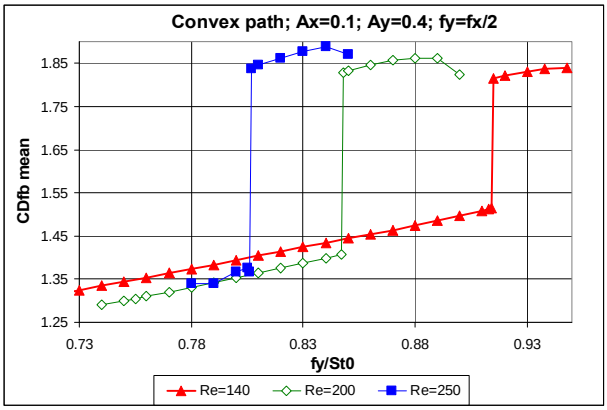

Figure 7. Time-mean of fixed body drag versus frequency ratio for Re=140, 200 and 250

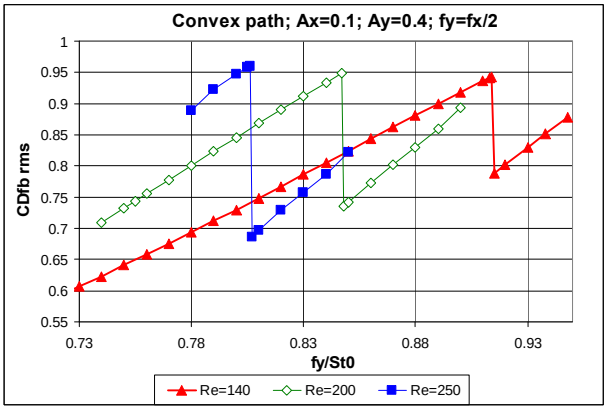

Figure 8. Rms of fixed body drag versus frequency ratio for Re=140, 200 and 250

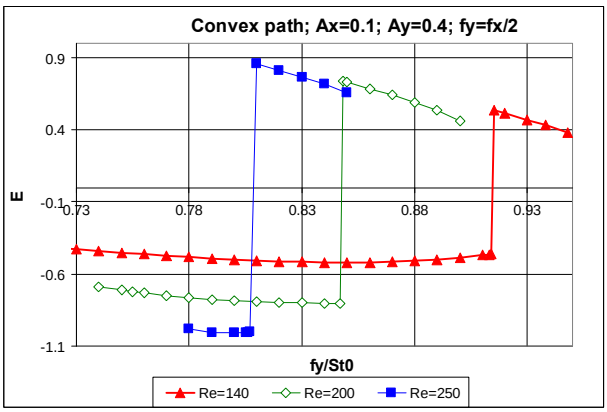

Figure 9. Mechanical energy transfer versus frequency ratio for Re=140, 200 and 250

Figure 10 shows the mechanical energy transfer due to transverse (E_1) and in-line (E_2) cylinder motions and the sum of these two (E), against frequency ratio for a fixed Re of 200. Before the jump all three E values are negative. After the jump E_2 increases suddenly to approximately zero at this Reynolds number, but since E_2 is approximately zero and E_1 becomes positive, the sum of these coefficients is positive.

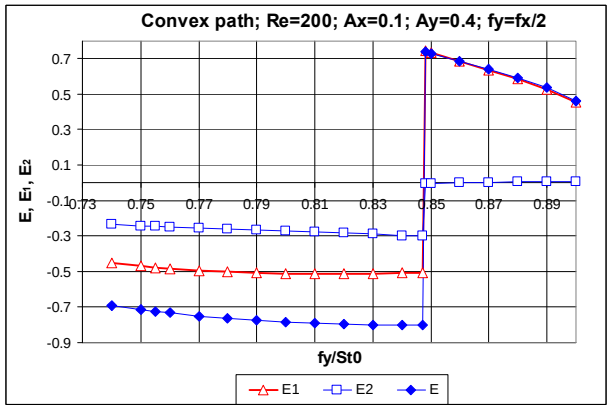

Figure 10. Mechanical energy transfer E_1, E_2 and E versus frequency ratio for Re=200

Pre- and Post-Jump Analysis The vicinity of a jump is investigated by different means, such as the time history of fixed body lift and drag, limit cycle curves and vorticity contours before and after a jump. The jump investigated here is the one for Re=200 and can be seen in Figs. 6 to 10. The pre- and post-jump frequency ratio values are $(f_y/St_0)_1$=0.847 and $(f_y/St_0)_2$=0.848.

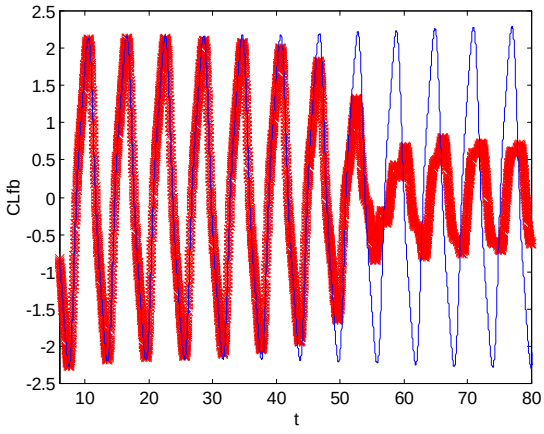

Figure 11. Time history of fixed body lift; transient part (thick line: f_y/St_0=0.847; thin line: f_y/St_0=0.848); Re=200

The time histories of the fixed body lift for the two frequency ratios are shown at the dimensionless time interval of [6, 80] in Fig. 11. Pre-jump curves will be denoted by thick lines and post-jump curves by thin lines throughout Figs. 11 to 14. As can be seen, the two time history curves coincide at beginning of the investigation, but then begin to diverge and both signals become periodic as shown in Fig. 12. There is just

a tiny difference between the frequency ratios but the obtained periodic fixed body lift coefficients are drastically different from each other. The periodic part of the time history of fixed body drag also differs substantially for the two cases shown in Fig. 13.

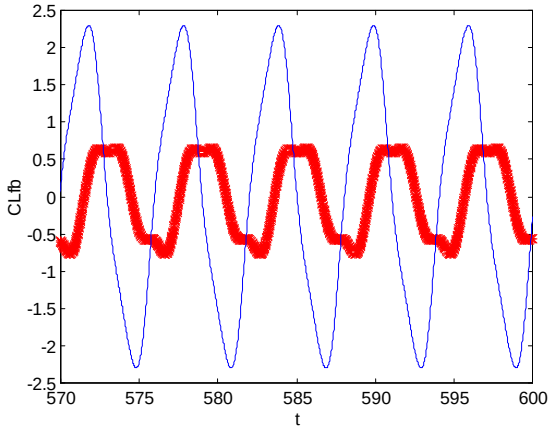

Figure 12. Time history of fixed body lift; periodic part (thick line: f_y/St_0=0.847; thin line: f_y/St_0=0.848); Re=200

Figure 14 shows the limit cycle curves ($C_{D\,fb}$,$C_{L\,fb}$) for the pre- and post-jump cases. Again, the very small difference in frequency ratio results in a drastic change in the shape of the two limit cycle curves, although here they are not mirror images of each other, as for the two sides of a jump for in-line cylinder oscillation (Baranyi, 2009; Baranyi et al., 2010).

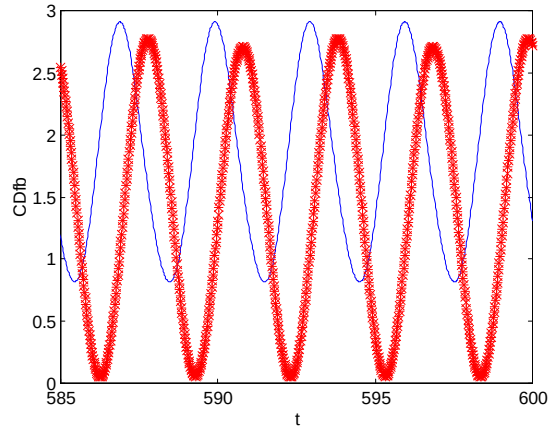

Figure 13. Time history of fixed body drag; periodic part (thick line: f_y/St_0=0.847; thin line: f_y/St_0=0.848); Re=200

Figure 15 shows the vorticity contours for the pre- and post-jump frequency ratio values of $(f_y/St_0)_1$=0.847 and $(f_y/St_0)_2$=0.848 belonging to the same cylinder positions (t=66T_y where T_y=1/f_y is the period based of f_y) for Re=200. The gray lines indicate negative vorticity values, rotating clockwise, and the black are positive, rotating counter-clockwise. A very small change in the oscillation frequency resulted in a substantial difference in the flow pattern. The pre-jump flow pattern shown in the top figure reveals a 2P (two pairs of vortices shed in a period) wake structure. The post-jump wake structure (bottom figure) is 2S (two single vortices). The post-jump wake structure is much narrower than the pre-jump one. Surprisingly, the higher TM of drag value belongs to the narrower wake (see Fig. 7).

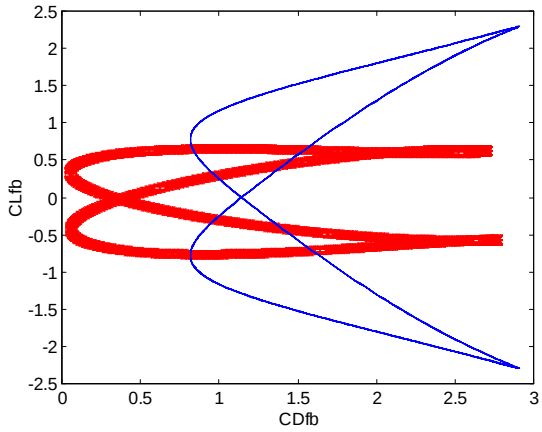

Figure 14. Limit cycle (C_{Dfb},C_{Lfb}); Re=200 (thick line: f_y/St_0=0.847; thin line: f_y/St_0=0.848)

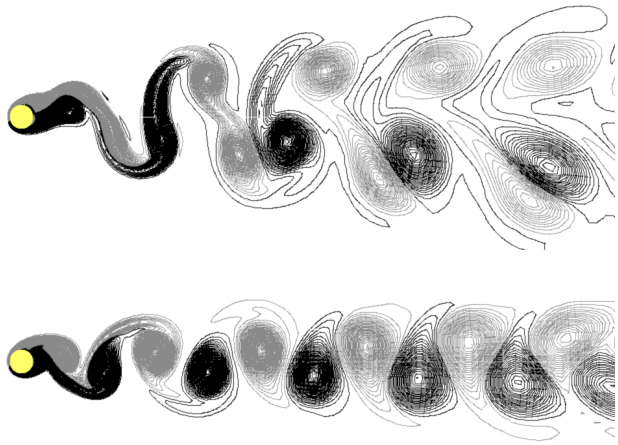

Figure 15. Pre- and post-jump vorticity contours; Re=200: top: f_y/St_0=0.847; bottom: f_y/St_0=0.848

Vorticity contours were investigated also for Re=140 and 250 for the pre- and post- jump frequency ratio values. The switch in the wake structures for all three Reynolds number was found to be very similar. Figure 16 shows the vorticity contours for Re=140 before and after the jump. The cylinder positions are the same for both contours. Again the wake becomes narrower and the pattern changes from 2P to 2S. The same trends were found for the convex case of Re=250, not shown here.

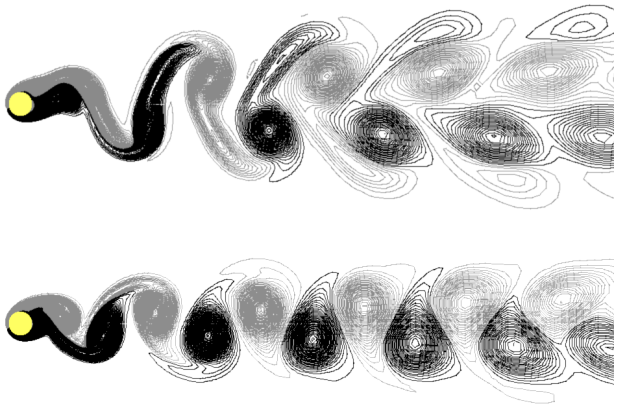

Figure 16. Pre- and post-jump vorticity contours; Re=140: top: f_y/St_0=0.914; bottom: f_y/St_0=0.915

Results for Concave Cylinder Paths

Now results for the concave cylinder path are shown as a function of the frequency ratio for the three Reynolds numbers. TM values of fixed body lift (not shown here) were very near to zero for all the computed cases. Figure 17 shows the rms of fixed body lift versus frequency ratio. The rms values increase with increasing f_y/St_0 values and a single jump can be found only at the highest Reynolds number of 250.

Figure 18 shows the TM values of fixed body drag against frequency ratio. The three curves represent similar drag values. A very small jump can be seen in the curve belonging to Re=250. The rms values of fixed body drag curves shows similar trends in Fig. 19: it increases with frequency ratio and larger rms values belong to larger Re values at a fixed frequency ratio. Again, a jump is discernable for Re=250.

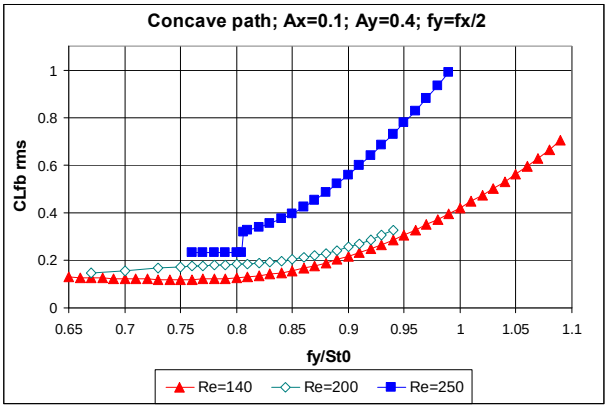

Figure 17. Rms of fixed body lift versus frequency ratio for Re=140, 200 and 250

Figure 20 shows the total mechanical energy transfer against frequency ratio. A jump can be found again in the Re=250 curve only. For Re=140 E is negative if f_y/St_0 is smaller than 0.84 and becomes positive above this value. For Re=200 this critical frequency ratio value where E changes its sign shifts to a smaller value of 0.78. For the highest Reynolds number all E values are positive, which would result in VIV in the corresponding case of free vibration.

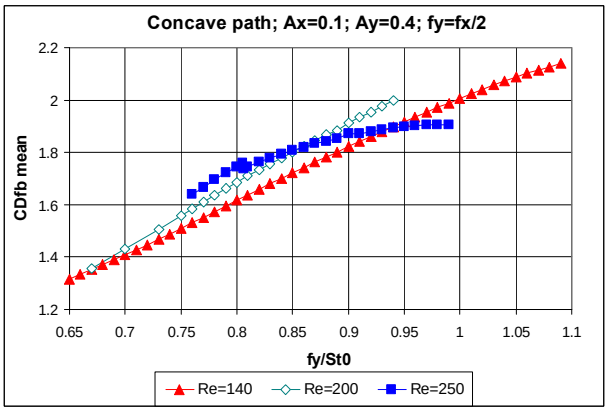

Figure 18. Time-mean of fixed body drag versus frequency ratio for Re=140, 200 and 250

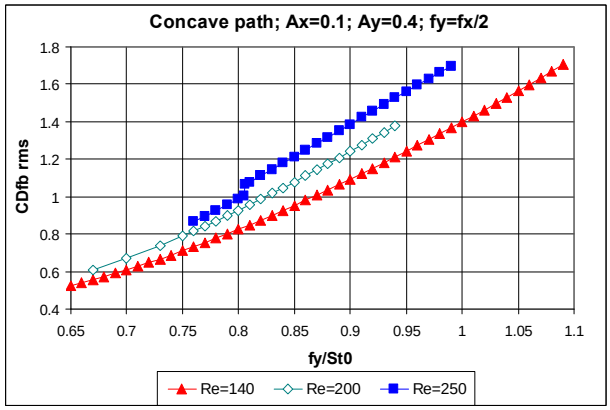

Figure 19. Rms of fixed body drag versus frequency ratio for Re=140, 200 and 250

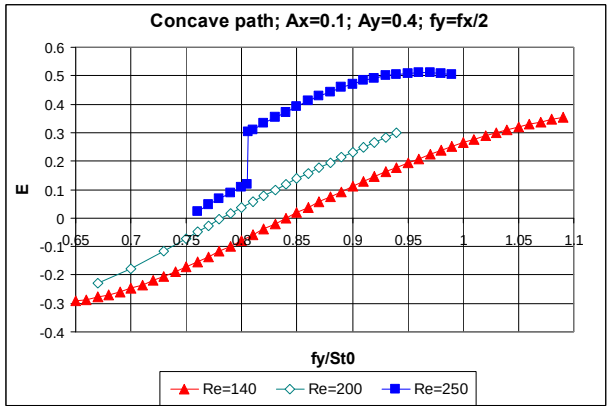

Figure 20. Mechanical energy transfer versus frequency ratio for Re=140, 200 and 250

Pre-and post jump analysis was carried out for the concave cylinder path at Re=250. Vorticity contours can be seen in Fig. 21 for f_y/St_0=0.805 and 0.806 at the same instant of t=400.

Again a tiny change in the frequency ratio resulted in a strong change in the vortex structure. The top figure (pre-jump) shows what appears to be a 2S-type vortex structure, while the bottom figure (post-jump) is P+S (a pair and a single vortex are shed in each cycle) in the near wake.

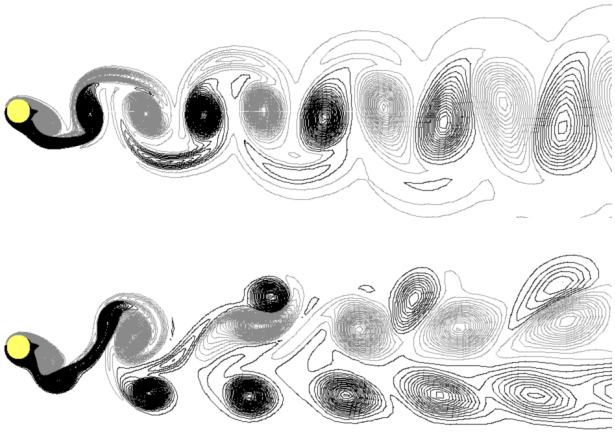

Figure 21. Pre- and post-jump vorticity contours; Re=250: top: f_y/St_0=0.805; bottom: f_y/St_0=0.806

CONCLUSIONS

This computational study deals with the systematic investigation of flow around a cylinder forced to follow either a convex or a concave arc at three Reynolds numbers of 140, 200 and 250 against frequency ratio f_y/St_0. The major findings are:

- Computations carried out for Re=140 for both type of cylinder motions for two substantially different size computational domains (R_2/R_1=60 and 360) compare well.
- When the time-mean and rms values are plotted against frequency ratio, the convex cylinder motion resulted in a single jump between the state curves for each every time-mean or rms curve for all three Reynolds numbers. The location of jumps are identical in curves belonging to the same Re values. By increasing Re the location of jumps shifts to smaller frequency ratio values.
- After a jump positive energy transfer values were obtained for all three Reynolds numbers. This could be dangerous for a freely vibrating cylinder.
- Pre- and post-jump analysis for the convex cylinder path at Re= 200 shows that a very small change in the value of the frequency ratio can result in a drastic change in the features of the flow. Vortex structure changed abruptly from 2P to 2S and the wake became narrower.
- Although probably less important in practice, the concave cylinder path resulted in a small jump only at Re=250. The energy transfer can be positive over a wide frequency ratio domain.

In this study only two phase angles (or cylinder paths) were investigated due to the huge amount of computational time involved. Further phase angle values and amplitude effect should be investigated in the future. Ideally, repeating the investigation for free cylinder motion can be achieved.

ACKNOWLEDGMENTS

The support provided by the Hungarian Research Foundation (OTKA Projects K 76085 and K 68207) is gratefully acknowledged. The author thanks Mr. L. Daróczy for designing the flow visualization software. The work was carried out as part of the TÁMOP-4.2.1.B-10/2/KONV-2010-0001 project in the framework of the New Hungarian Development Plan. The realization of this project is supported by the European Union, co-financed by the European Social Fund.

REFERENCES

Al-Mdallal, Q.M., Lawrence, K.P. and Kocabiyik, S., 2007, "Forced streamwise oscillations of a circular cylinder: Locked-on modes and resulting fluid forces," *Journal of Fluids and Structures* **23**, 681-701.

Baranyi, L., 2003, "Computation of unsteady momentum and heat transfer from a fixed circular cylinder in laminar flow," *Journal of Computational and Applied Mechanics* **4**, 13-25.

Baranyi, L., 2005, "Lift and drag evaluation in translating and rotating non-inertial systems," *Journal of Fluids and Structures* **20**(1), 25-34.

Baranyi, L., 2008, "Numerical simulation of flow around an orbiting cylinder at different ellipticity values," *Journal of Fluids and Structures* **24**, 883-906.

Baranyi, L., 2009, "Sudden and gradual alteration of amplitude during the computation for flow around a cylinder oscillating in transverse or in-line direction," *ASME 2009 Pressure Vessels and Piping Conference, Symposium on Flow-Induced Vibration*. Prague, Paper No. PVP2009-77463.

Baranyi, L., 2010, "Numerical simulation of the flow around a circular cylinder following a figure-8-like path," *Proc. 7th International Symposium on Fluid-Structure Interactions, Flow-Sound Interactions, and Flow-Induced Vibration and Noise,* (*within FEDSM2010-ICNMM2010 ASME Conference 2010*), Montreal, Québec, Canada, (2010), on CD ROM, pp. 1-7, Paper No. FEDSM-ICNMM2010-30888

Baranyi, L., Huynh, K. and Mureithi, N.W., 2010, "Dynamics of flow behind a cylinder oscillating in-line for low Reynolds numbers," Proc. *7th International Symposium on Fluid-Structure Interactions, Flow-Sound Interactions, and Flow-Induced Vibration and Noise,* Montreal, Québec, Canada, on CD ROM, pp. 1-10, Paper No. FEDSM-ICNMM2010-31183

Blackburn, H.M. and Henderson, R.D., 1999, "A study of two-dimensional flow past an oscillating cylinder," *Journal of Fluid Mechanics* **385**, 255-286.

Cetiner, O. and Rockwell, D., 2001, "Streamwise oscillations of a cylinder in a steady current. Part 1. Locked-on states of vortex formation and loading," *Journal of Fluid Mechanics* **427**, 1-28.

Crawford, J.D. and Knobloch, E., 1991, "Symmetry and symmetry-breaking bifurcations in fluid dynamics," *Annual Review of Fluid Mechanics* **23**, 341-387.

Didier, E. and Borges, A.R.J., 2007, "Numerical predictions of low Reynolds number flow over an oscillating circular cylinder," *Journal of Computational and Applied Mechanics* **8**(1), 39-55.

Flemming, F. and Williamson, C.H.K., 2005, "Vortex-Induced Vibration of a Pivoted Cylinder," *Journal of Fluid Mechanics* **522**, 215–252.

Jauvtis, N. and Williamson, C. H. K., 2004, "The Effect of Two Degrees of Freedom on Vortex-Induced Vibration and at Low Mass and Damping," *Journal of Fluid Mechanics* **509**, 23–62.

Jeon, D. and Gharib, M., 2001, "On circular cylinders undergoing two-degree-of-freedom forced motions," *Journal of Fluids and Structures* **15**, 533-541.

Kaiktsis, L., Triantafyllou, G.S. and Özbas, M., 2007, "Excitation, inertia, and drag forces on a cylinder vibrating transversely to a steady flow," *Journal of Fluids and Structures* **23**, 1-21.

Kheirkhah, S. and Yarusevych, S., 2010, "Two-degree-of-freedom flow-induced vibrations of a circular cylinder with a high moment of inertia ratio," *Proc. ASME 2010 3rd Joint US-European Fluids Engineering Summer Meeting and 8th Int. Conference on Nanochannels, Microchannels, and Minichannels (FEDSM-ICNM2010)*, Montreal, Québec, Canada, (2010), on CD ROM, pp. 1-10, Paper No. FEDSM-ICNMM2010-30042.

Leong, C.M. and Wei, T., 2008, "Two-Degree-of-Freedom Vortex-Induced Vibration of a Pivoted Cylinder below Critical Mass Ratio," *Proc. R. Soc. A.* **464**, 2907-2927.

Lu, X.Y. and Dalton, C., 1996, "Calculation of the timing of vortex formation from an oscillating cylinder," *Journal of Fluids and Structures* **10**, 527-541.

Mureithi, N.W., Huynh, K., Rodriguez, M. and Pham, A., (2010), "A simple low order model of forced Karman wake" *International Journal of Mechanical Sciences* **52**(11), 1522-1534.

Peppa, S., Kaiktsis, L. and Triantafyllou, G.S., 2010, "The effect of in-line oscillation on the forces of a cylinder vibrating in a steady flow," *Proc. 7th International Symposium on Fluid-Structure Interactions, Flow-Sound Interactions, and Flow-Induced Vibration and Noise,* (*within FEDSM2010-ICNMM2010 ASME Conference 2010*), Montreal, Québec, Canada, (2010), on CD ROM, pp. 1-8, Paper No. FEDSM-ICNMM2010-30054

Posdziech, O. and Grundmann, R., 2007, "A systematic approach to the numerical calculation of fundamental quantities of the two-dimensional flow over a circular cylinder," *Journal of Fluids and Structures* **23**, 479-499.

Prasanth, T.K. and Mittal, S., 2009, "Flow-induced oscillation of two circular cylinders in tandem arrangement at low Re," *Journal of Fluids and Structures* **25**, 1029-1048.

Sanchis, A., Sælevik, G., Grue, J., 2008, "Two-degree-of-freedom vortex-induced vibrations of a spring-mounted rigid cylinder with low mass ratio," *Journal of Fluids and Structures* **24**, 907-919.

Williamson, C.H.K. and Roshko, A., 1988, "Vortex formation in the wake of an oscillating cylinder," *Journal of Fluids and Structures* **2**, 355-381.

Williamson, C.H.K., 2004, "Vortex-Induced Vibrations," *Annual Review of Fluid Mechanics* **36**, 413-455.

